AGU PUBLICATIONS

JGR

Journal of Geophysical Research: Atmospheres

RESEARCH ARTICLE
10.1002/2017JD027522

Key Points:
- Plantation forest is cooler in the daytime and mostly warmer at night than an adjacent shrub land in Inner Mongolia, China
- Energy balance closure is an important condition for partitioning of biophysical effects of land use change
- Biophysical contributions from the surface temperature decomposition metric theory are an order of magnitude greater than the related terms from the intrinsic biophysical mechanism theory

Supporting Information:
- Supporting Information S1

Correspondence to:
X. Lee and G. Lin,
xuhui.lee@yale.edu;
lingh@tsinghua.edu.cn

Citation:
Wang, L., Lee, X., Schultz, N., Chen, S., Wei, Z., Fu, C., … Lin, G. (2018). Response of surface temperature to afforestation in the Kubuqi Desert, Inner Mongolia. *Journal of Geophysical Research: Atmospheres*, *123*, 948–964. https://doi.org/10.1002/2017JD027522

Received 27 JUL 2017
Accepted 13 JAN 2018
Accepted article online 17 JAN 2018
Published online 29 JAN 2018

Response of Surface Temperature to Afforestation in the Kubuqi Desert, Inner Mongolia

Liming Wang[1,2,3], Xuhui Lee[2,4], Natalie Schultz[2], Shiping Chen[5], Zhongwang Wei[2,4], Congsheng Fu[2,4], Yunqiu Gao[2,4], Yanzheng Yang[1,3], and Guanghui Lin[1,3]

[1]Ministry of Education Key Laboratory for Earth System Modeling, Department of Earth System Science, Tsinghua University, Beijing, China, [2]School of Forestry and Environmental Studies, Yale University, New Haven, CT, USA, [3]Division of Ocean Science and Technology, Graduate School at Shenzhen, Tsinghua University, Shenzhen, China, [4]Yale-NUIST Center on Atmospheric Environment, Nanjing University of Information Science and Technology, Nanjing, China, [5]State Key Laboratory for Vegetation Ecology, Institute of Botany, Chinese Academy of Sciences, Beijing, China

Abstract In this study, micrometeorological observations in a shrub ecosystem and an adjacent poplar plantation forest ecosystem in the Kubuqi Desert, Inner Mongolia, China, are used to evaluate the theory of intrinsic biophysical mechanism (IBPM) and to investigate the biophysical effects of afforestation. Results indicate that after forcing energy balance closure to the observed fluxes, the IBPM theory agrees very well with the observed temporal variations in the surface temperature and with the observed temperature difference between the paired sites at the half-hourly time scale. Afforestation activity in this dryland landscape has a cooling effect (−0.5 ± 0.2 K) in the daytime in all the seasons and a warming effect (0.2 ± 0.1 K) in the nighttime during the winter, spring and, autumn but a cooling effect (−1.0 ± 0.3 K) in the summer at night. These temperature changes are decomposed into contributions from changes in surface albedo, surface roughness, Bowen ratio, and ground heat flux. Comparison is made between the IBPM theory and the theory of the decomposed temperature metric.

1. Introduction

The influence of forest management on the climate system can be evaluated in terms of their carbon sequestration potential or biogeochemical effect (Holtsmark, 2012; Hudiburg et al., 2011) and biophysical forcings (Bonan, 2008; Bright et al., 2014; Davin & de Noblet-Ducoudre, 2010; Mahmood et al., 2014). The biophysical contributions to the climate system include the exchanges of energy, water, and momentum between the Earth's surface and the lower atmosphere. Unlike the biogeochemical effect, the biophysical processes are dependent on regional climate conditions. For example, albedo change dominates the biophysical effect of deforestation in the boreal zone, especially in the winter because of snow cover and a land albedo-sea ice feedback (Bonan et al., 1992; Davin & de Noblet-Ducoudre, 2010). In tropical climate, the role of albedo change is minor, and evapotranspiration change plays a major role in determining the overall deforestation climatic impact (Bala et al., 2007). Changes in surface roughness appear to be more important in humid climates than in dry climates, because of its influence on sensible heat dissipation and on the latent heat flux (Bright et al., 2017; Burakowski et al., 2018; Lee et al., 2011; Rigden & Li, 2017). Because of this regional context, the same land management regime will have very different climate consequences in different climate zones. The ability to partition the overall biophysical effect to these component contributions constitutes an integral part of climatic evaluation of land management.

Currently, there are two main theories for isolating the contributions to changes in surface temperature from individual biophysical factors of land use change. The first theory, termed the direct decomposed temperature metric (DTM) theory, was first proposed by Juang et al. (2007) and later refined by Luyssaert et al. (2014). The DTM theory attributes changes in the surface temperature due to differences in surface albedo, incoming radiation, ground heat flux, and sensible and latent heat flux between two land use classes. The temperature perturbation is a direct consequence of the surface energy balance and linearization of the Stephan-Boltzmann expression for the surface outgoing longwave radiation.

The second theory, termed the intrinsic biophysical mechanism (IBPM) theory, was first proposed by Lee et al. (2011) to investigate the local climate effect of deforestation and later modified by Zhao et al. (2014) to quantify surface temperature responses to urbanization. According to this theory, changes in

the surface temperature in response to land use changes are consequences of the local longwave radiative feedback at the surface and energy redistribution brought by changes to the aerodynamic resistance and surface evaporation.

These theories can be used for diagnostic or prognostic calculations. In a diagnostic application, all variables needed for the partitioning calculation are provided either by field measurements or as model outputs; no parameterizations are involved. Zhao et al. (2014) and Chen and Dirmeyer (2016) provided two examples of diagnostic application in the investigation of urban heat islands and the biophysical effect of land cover change, respectively. In a prognostic application, the resistance to heat diffusion in the IBPM theory is predicted with a set of parameterization equations. For example, Lee et al. (2011) calculated the total heat diffusion resistance by combining a standard Monin-Obukhov formulation for the aerodynamic resistance with a formulation for the radiometric resistance. In a study on the biophysical effects of alternative forest management in Norway, Bright et al. (2014) calculated the heat resistance using a formulation for neutral conditions.

Chen and Dirmeyer (2016) have compared the DTM and IBPM theories with observations made at eight paired FLUXNET sites. They found that surface temperature changes between open lands and forests calculated with the DTM theory are in agreement with the observed temperature changes, and after adjusting for air temperature differences between the paired sites, the results of IBPM are also in agreement with the observations.

The published studies cited above focus on seasonal and annual mean behaviors. Even though both theories are based on the principle of surface energy balance at a short time scale (hourly), few studies have examined the validity of these theories at this time scale (hourly) against field observations except for Burakowski et al. (2018), who have evaluated the original IBPM against observations at temperate humid sites.

Afforestation in semiarid areas is an important form of land use change (Chirino et al., 2006; Grunzweig et al., 2007; Nosetto et al., 2006; Sartori et al., 2007). In China, multiple afforestation programs have been launched since 1978, including the "Three North" Shelterbelt Development Program (Li et al., 2012), the Beijing-Tianjin Sand Source Control Program (Wu et al., 2013), the Nature Forest Conservation Program, and the Grain-to-Green Program (Jia et al., 2014; Zhang et al., 2016). These programs focus on local environment restoration by planting trees and by protecting natural forests in semiarid and arid regions. Now, China has the largest afforested area in the world (about 69 million hectares in 2013) (State Forestry Administration of the People's Republic of China, 2013), and the area of planted forest has been increasing by 1.7 million hectares per year during the last 20 years (Peng et al., 2014). The afforestation increases carbon sequestration and also alters local biophysical properties, which have the potential to influence regional climates. Peng et al. (2014) evaluated the influence of afforestation on local land surface temperature for China. Their results showed that in semiarid areas, compared with adjacent grasslands or croplands, forests have a cooling effect in the daytime and a warming effect in the nighttime. This large-scale, remote sensing study highlights the role of afforestation on surface temperature. However, it is not clear as to which of the biophysical factors contributes the most to the surface temperature changes.

In this study, we investigated the biophysical effect of afforestation in the Kubuqi Desert, Inner Mongolia, China, using micrometeorological observations made in a shrub ecosystem and an adjacent plantation forest ecosystem. We aim (1) to evaluate the performance of the IBPM theory for predicting the surface temperature changes over time and changes associated with the land use difference, (2) to quantify the contributions of radiative forcing, surface roughness, evaporation, and ground heat flux to surface temperature change (ΔT_s) over the diurnal and seasonal cycles, and (3) to compare the ΔT_s decomposition results obtained with the IBPM and the DTM theory.

2. Theoretical Frameworks

2.1. DTM

The surface energy balance equation is

$$S + L_{\downarrow} - \sigma T_s^4 = R_n = H + \mathrm{LE} + G \tag{1}$$

where S is net surface shortwave radiation, $L_{\downarrow}$ is incoming longwave radiation, σ is the Stephan-Boltzmann constant, T_s is surface temperature, R_n is net radiation, H is sensible heat flux, LE is latent heat flux, and G is

ground heat flux. The net shortwave radiation is given by $S = (1 - \alpha)\, K_{\downarrow}$, where α is surface albedo and $K_{\downarrow}$ is solar radiation flux incident on the surface.

According to Juang et al. (2007) and Luyssaert et al. (2014), change to the surface temperature brought by land use change can be expressed as

$$\Delta T_s = T_s - T_s \approx \frac{1}{4T_s^3}\left(T_s^4 - T_s^4\right) = \lambda_0 \Delta S + \lambda_0 \Delta L_{\downarrow} - \lambda_0(\Delta LE + \Delta H) - \lambda_0 \Delta G \tag{2}$$

(details are in the supporting information) where T_s and T_s represents the surface temperature of an open land (shrubland in this study) and a forest, respectively, Δ denotes the difference in a variable between the open land and the forest, and λ_0 is given by

$$\lambda_0 = \frac{1}{4\sigma T_s^3} \tag{3}$$

and is referred to by Lee et al. (2011) as the local climate sensitivity. The first term on the right-hand side of equation (2) represents shortwave radiative forcing associated with albedo change, the second term represents longwave radiative forcing, the third term represents changes in sensible heat and latent heat flux, and the fourth term represents changes in the ground heat flux.

Equation (2) is a direct consequence of linear approximation to the longwave radiation term (the third term on the left-hand side of equation (1)). The original theory includes three more terms: change in incoming shortwave radiation, change in surface emissivity, and a residual flux term (Luyssaert et al., 2014). We ignored the first two additional terms, on the approximation that the incoming shortwave radiation and surface emissivity are the same between the two sites. We did not explicitly consider the residual flux term but instead distributed it to the sensible heat and latent heat fluxes by forcing energy balance closure (details in section 4).

To be consistent with the convention in the published literature, we define the surface temperature difference ΔT_s as the temperature of the open shrubland minus the temperature of the plantation forest, which is a measure of deforestation effect on the surface climate. The effect of afforestation should be interpreted as $-\Delta T_s$ or as having the opposite sign to the deforestation effect.

2.2. IBPM

The IBPM theory is also based on the surface energy balance principle (equation (1)). In addition to using the linear approximation to the longwave radiation term, it accounts for the fact that H and LE are implicit functions of the surface temperature in the differentiation of the surface energy balance equation. By expressing H using a resistance formula and by introducing Bowen ratio, Lee et al. (2011) obtain a solution for T_s,

$$T_s = \frac{\lambda_0}{1+f}\left(R_n^* - G\right) + T_a \tag{4}$$

where T_a is air temperature (K), R_n^* is apparent net radiation

$$R_n^* = S + L_{\downarrow} - \sigma T_a^4 \tag{5}$$

and the energy redistribution factor f is given by

$$f = \frac{\rho C_p}{4 r_t \sigma T_s^3}\left(1 + \frac{1}{\beta}\right) \tag{6}$$

where ρ is air density (kg m^{-3}), C_p is specific heat of air at constant pressure (J kg^{-1} K^{-1}), β is Bowen ratio ($\beta = H/LE$), and r_t is total heat transfer resistance (s m^{-1}).

In a diagnostic application, r_t is calculated by definition,

$$r_t = \rho C_p \frac{T_s - T_a}{H} \tag{7}$$

where variables on the right-hand side are provided by field observations.

In a prognostic application, r_t is calculated with a set of parameterization equations using micrometeorological variables as inputs. Specifically,

$$r_t = r_a + r_{ex} + r_r \tag{8}$$

where r_a is the aerodynamic resistance, r_{ex} is the excess resistance, and r_r is the radiometric resistance. The first two resistances are given by

$$r_a = \frac{\left[\ln\left(\frac{z-d}{z_0}\right) - \Psi_M\right]\left[\ln\left(\frac{z-d}{z_0}\right) - \Psi_H\right]}{k^2 u} \tag{9}$$

$$r_{ex} = \frac{\ln\left(\frac{z_0}{z_h}\right)}{k u^*} \tag{10}$$

where k is the von Karman constant, u is wind speed, z is the measurement height of air temperature and wind speed, d is the displacement height, z_0 is the aerodynamic roughness length, z_h is the thermal roughness length, u_* is the friction velocity, and Ψ_M and Ψ_H are the stability correction functions for momentum and heat, respectively (Lhomme et al., 1988; Stewart et al., 1994). No standard parameterization for r_r exists in the published literature. In this study, we used a combination of the parameterization given by Zhao et al. (2016) and our own formulation (section 4).

The contributions of individual biophysical factors to ΔT_s are obtained by differentiating equation (4), as

$$\Delta T_s \approx \frac{\lambda_0}{1+f}\left(\Delta S + \Delta L_\downarrow\right) + \frac{-\lambda_0}{(1+f)^2}\left(R_n^* - G\right)\Delta f + \frac{-\lambda_0}{1+f}\Delta G + \left(\Delta T_a - \frac{\lambda_0}{1+f}\sigma \Delta T_a^4\right) \tag{11}$$

where Δ again denotes the difference in a variable between the open land and the forested land, and Δf is the change in the energy redistribution factor, which is further attributed to changes in surface roughness (Δf_1) and in Bowen ratio (Δf_2):

$$\Delta f_1 = \frac{-\rho C_p}{4 r_t \sigma T_s^3}\left(1 + \frac{1}{\beta}\right)\frac{\Delta r_t}{r_t} \tag{12}$$

$$\Delta f_2 = \frac{-\rho C_p}{4 r_t \sigma T_s^3}\left(\frac{\Delta \beta}{\beta^2}\right) \tag{13}$$

The expanded form of equation (11) is given as

$$\Delta T_s \approx \frac{\lambda_0}{1+f}\left(\Delta S + \Delta L_\downarrow\right) + \frac{-\lambda_0}{(1+f)^2}\left(R_n^* - G\right)\Delta f_1 + \frac{-\lambda_0}{(1+f)^2}\left(R_n^* - G\right)\Delta f_2 + \frac{-\lambda_0}{1+f}\Delta G + \left(\Delta T_a - \frac{\lambda_0}{1+f}\sigma \Delta T_a^4\right) \tag{14}$$

where Term 1 on the right-hand side of the equation represents the radiative forcing effect, Terms 2 and 3 represents the role of energy redistribution associated with roughness change and with Bowen ratio change, respectively, Term 4 represents ground heat flux change, and Term 5 is related to air temperature change.

Equation (14) is a modified version of the original IBPM theory. In Lee et al. (2011), the air temperature and the incoming longwave radiation are assumed to be measured at the blending height in the boundary layer and are therefore identical between the paired sites. In the present study, the incoming shortwave radiation was nearly identical (206.6 W m^{-2} at the forest site and 206.7 W m^{-2} at the shrub site over the 40 day study periods), but the longwave radiation was slightly different between the shrubland and the plantation forest. Some of the surface temperature difference observed between the paired sites can be attributed to the difference in $L_\downarrow$ (Term 1). Additionally, in our application of the IBPM theory, because the air temperature was measured at the screen height instead of the blending height, we cannot assume that T_a is identical between the two sites. Term 5 of equation (14) is meant to account for the difference in T_a.

In equation (14), the incoming longwave radiation changes are combined into Term 1 to make the analysis more concise. Because the influence of incoming longwave radiation can be ignored in the daytime (section 5.2), Term 1 is essentially the radiative forcing (albedo) effect. In the nighttime, the influence of albedo is 0, and Term 1 gives the influence of incoming longwave radiation.

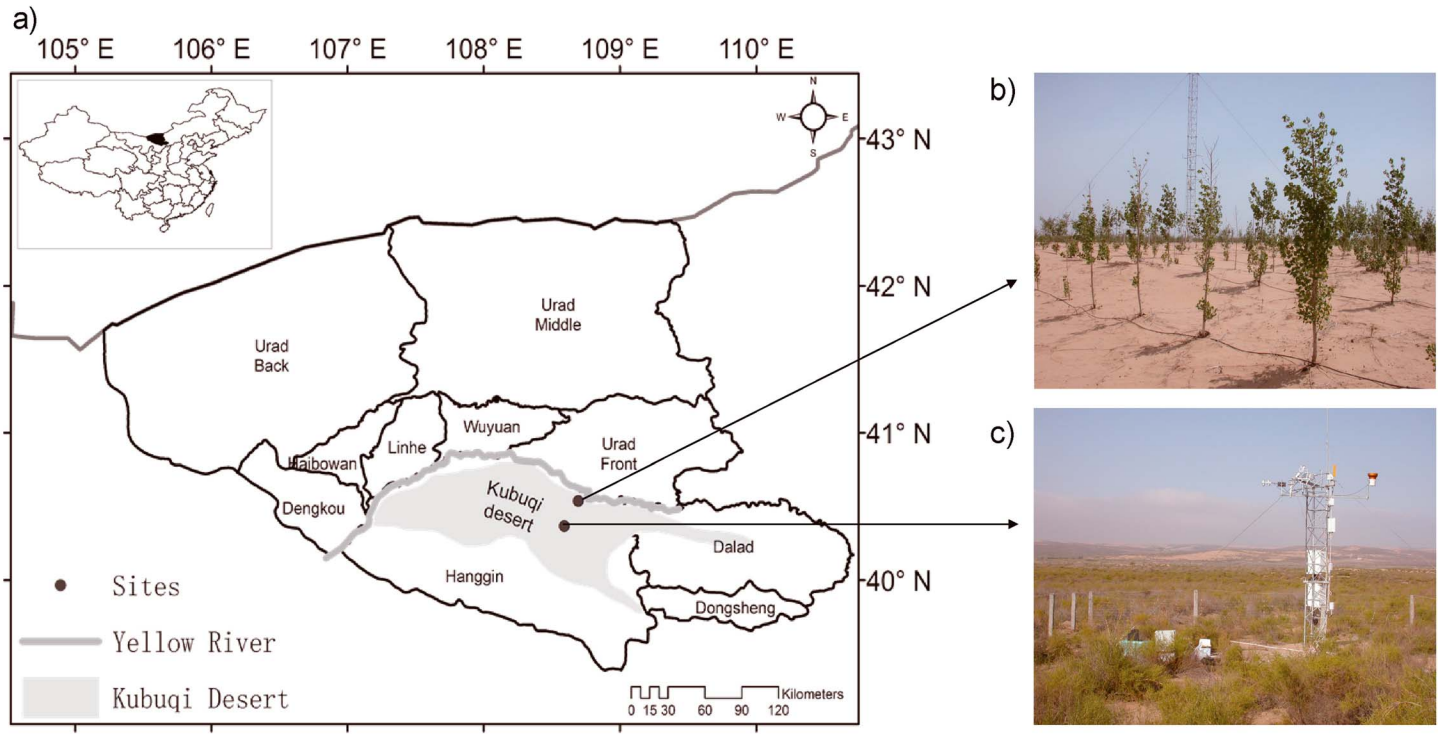

Figure 1. (a) Locations and (b, c) pictures of the study sites. Figure 1b is the poplar plantation, and Figure 1c is the native shrubland. The photos were taken in 2006.

3. Site Description and Data

The Kubuqi Desert, the seventh largest desert in China, is a major sand source that affects air quality in Inner Mongolia and the Beijing municipality. To reduce desertification and control dust storms, local governments and private sectors have been planting fast-growing and high-yielding commercial forests (*Populus* spp.) in this region since 1988. By the end of 2014, the total area of plantation forests was 1,361 km^2 (Elion Company, personal communication, 2016). To evaluate the ecological benefits of afforestation, we established two eddy flux sites in an afforested poplar ecosystem and a natural shrubland (*Artemisia ordosica*) ecosystem in the center of the Kubuqi Desert (40°32′N, 108°41′E, 1,020 m (poplar) and 1,160 m (shrub) above the mean sea level, Figure 1). The eddy covariance (EC) data and micrometeorology data were collected from January 2006 to December 2008. The distance between the two sites is 18 km. Monthly mean air temperature is −11°C in January and 24°C in July, and the annual mean precipitation is 318 mm according to the weather data from 1957 to 2000. The soil texture is arenosol. At the shrubland site, the average shrub coverage was 20% and average canopy height was 0.5 m. At the forest plantation site, the average canopy height was 3.0 m in 2006, the third year after afforestation. The trees were 6 years old, after having grown for 3 years before transplanting. This age class is typical of plantation forests in this region.

Each of the two sites was equipped with an EC system consisting of an open-path infrared gas analyzer (LI-7500, Li-Cor, Lincoln, NE, USA) and a sonic anemometer/thermometer (CSAT3, Campbell Scientific Inc., Logan, USA). The EC measurement height was 2.5 m at the shrubland site and 10.0 m at the plantation forest. The EC signals were recorded at 10 Hz by a datalogger (CR5000, Campbell Scientific Inc.), and eddy fluxes of sensible heat, water vapor, momentum, and CO_2 were computed at 30 min intervals. Coordinate rotation was performed according to the planar fit method (Wilczak et al., 2001), and WPL (Webb E K, Pearman G I, Leuning R) density corrections were applied to the fluxes (Webb et al., 1980).

Air temperature was recorded at three heights (1.5 m, 2.5 m, and 4.0 m at the shrubland site and 3.0 m, 6.0 m, and 10.0 m at the forest plantation site) with HMP45AC probes (Vaisala, Helsinki, Finland). Soil water content was measured using CS616 probes (Campbell Scientific, Inc.) at depths of 10, 20, 30, and 50 cm at both sites. Net radiation was measured with Q-7.1 net radiometers (Radiation and Energy Balance Systems, Inc., REBS,

Table 1
Energy Balance Closure at Forest Site and Shrub Site

Site	Season	EBR	Slope	Intercept (W m^{-2})	R^2
Forest	Winter	0.82	0.70 ± 0.10	7.53 ± 6.35	0.75
	Spring	1.02	0.77 ± 0.12	27.8 ± 7.20	0.91
	Summer	1.16	0.93 ± 0.09	28.7 ± 9.81	0.95
	Autumn	0.98	0.72 ± 0.11	8.74 ± 9.40	0.94
Shrub	Winter	1.09	1.02 ± 0.10	3.85 ± 13.12	0.85
	Spring	1.23	1.10 ± 0.11	10.87 ± 14.21	0.84
	Summer	1.12	0.96 ± 0.10	20.8 ± 3.18	0.78
	Autumn	1.04	0.84 ± 0.11	8.73 ± 4.51	0.92

Note. EBR is calculated by EBR $= \frac{\sum (H+\mathrm{LE})}{\sum (R_n - G)}$. Regression parameters are calculated based on half-hour results (geometric mean regression ± 1 standard error).

Bellevue, WA, USA) at the height of 4.0 m at the shrubland site and at the height of 10.0 m at the forest site. Soil heat flux was measured with three soil heat plates (HFT-3, REBS) at a depth of 3 cm.

This study focuses on four 10 day time sequences in 2006, including a winter period (day of year or DOY 45–54), a spring period (DOY 133–142), a summer period (DOY 215–224), and an autumn period (DOY 301–310). Half-hour air temperature, air density, energy flux components, and radiative data were used. These 10 day time sequences were selected because the missing sensible heat flux data are less than 10% in each period and the time intervals between adjacent periods are close to the length of one season (90 days).

4. Data Analysis

The surface temperature T_s was determined from the outgoing longwave radiation flux $L_\uparrow$ and corrected for the surface reflection of the downward longwave radiation flux, as

$$T_s = \left(\frac{L_\uparrow - (1-\varepsilon)L_\downarrow}{\varepsilon\sigma}\right)^{\frac{1}{4}} \quad (15)$$

where ε is surface emissivity (assumed to be 0.98 here) (Zhao et al., 2016).

The energy balance ratios (EBR) and regression parameters between the available energy ($R_n - G$) and the sum of latent and sensible heat fluxes (LE + H) are shown in Table 1. The mean energy imbalance is on the order of 5% but differed among the seasons. To constrain the energy balance, we calculated the imbalance term by terms on the left-hand side minus terms on the right-hand side of equation (1) and distributed the imbalance term to the sensible and latent heat fluxes in proportion to the measured Bowen ratio (Twine et al., 2000). The sensible and latent heat flux after this adjustment are denoted as H' and LE$'$. This adjustment was done at half-hourly intervals. In this analysis, we have ignored the canopy heat storage.

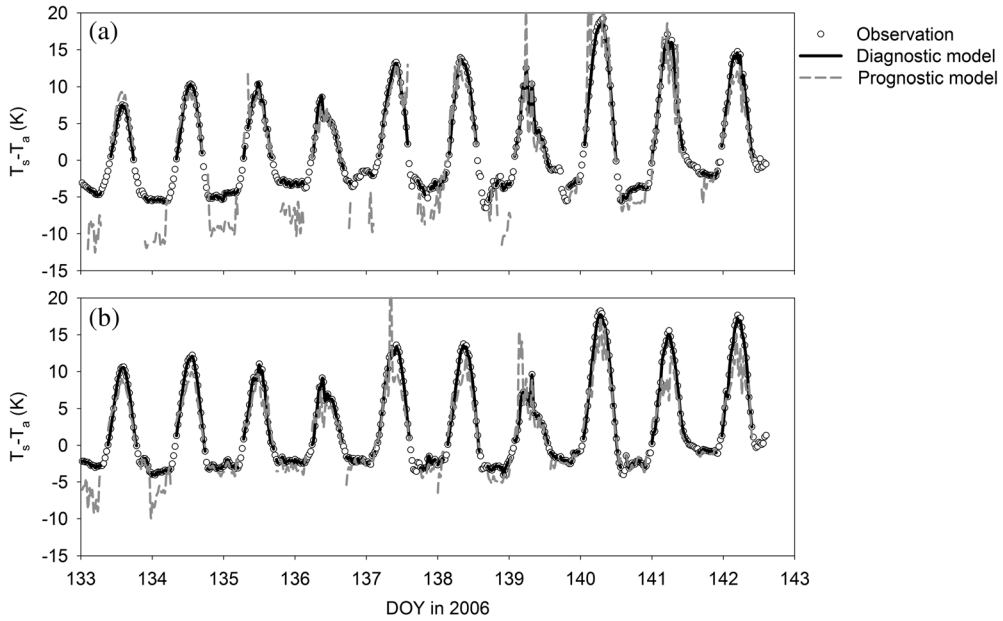

Figure 2. Differences between surface temperature and air temperature at (a) forest site and (b) shrub site in the spring. Dot represents the observations, black solid line represents result of diagnostic model, and gray dashed line represents result of prognostic model. Horizontal axis is DOY in 2006. Each data point represents one half-hourly observation.

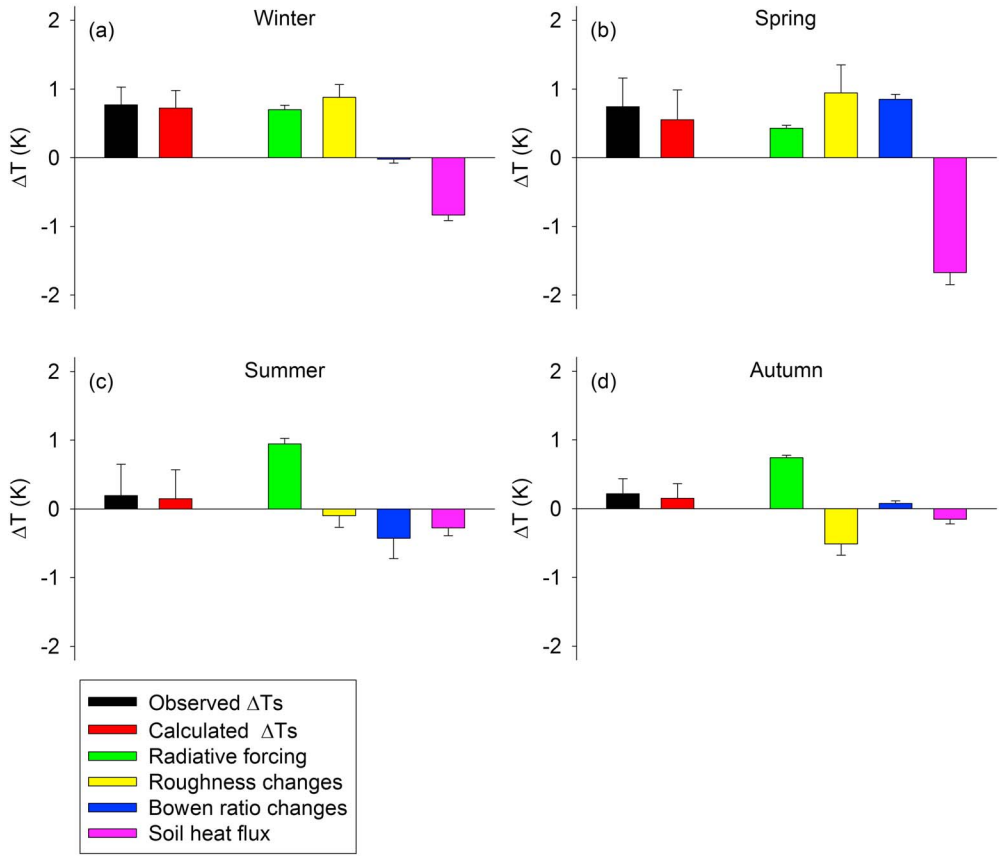

Figure 3. Partition of the daytime biophysical effect in different seasons according to the IBPM theory. Error bars are given as 1 SE. Black bars denote observed ΔT_s, red bars denote the ΔT_s calculated by the IBPM theory, green bars denote radiative forcing, yellow bars denote energy distribution associated with changes in roughness, blue bars denote energy distribution associated with changes in Bowen ratio, and pink bars denote the soil heat flux changes. The ΔT_s is the temperature of the open shrubland minus the temperature of the plantation forest (here and hereafter).

The principle of energy balance is the foundation for both the DTM and the IBPM theory, because the partitioning equations (equations (2) and (14)) are derived from the energy balance equation (equation (1)). If we do not force energy balance closure, the calculated ΔT_s will greatly diverge from the observation. The importance of energy balance closure is discussed in section 5.7.

In the diagnostic calculation using the IBPM theory, the total resistance r_t was determined using equation (7), where H was measured with EC and adjusted for energy balance closure; surface temperature T_s was determined using equation (15); and air temperature was measured with a thermometer at the height of 4.0 m and 10.0 m above the ground at the shrubland and the forest site, respectively.

In the prognostic calculation, the total resistance was determined using equation (8). The first two resistances (r_a and r_{ex}) were given by equations (9) and (10). The four height parameters (z, d, z_0, and z_h) are shown in Table S1, u and u_* were available from direct tower measurements, and the stability correction factors Ψ_M and Ψ_H were calculated according to the Businger-Dyer formulation (Businger, 1988). In unstable conditions (daytime), the radiometric resistance (r_r) was calculated with an exponential function of leaf area index (LAI; Zhao et al., 2016; Table S1). The LAI data came from 4 day global 500 m LAI product of MODIS (Moderate-Resolution Imaging Spectroradiometer, MCD15A3H) and was calibrated by intermittent site measurements. The LAI varied in the range of 0.10–0.58 at the shrubland site and 0.10–0.29 at the forest site. In stable conditions (nighttime), the formulation using constant values for each season provided by Zhao et al. (2016) does not work well. Therefore, we developed our own empirical parameterization. We first calculated the actual r_t using equation (7) and determined r_r as $r_r = r_t - (r_a + r_{ex})$, where r_a and r_{ex} were given by equations (9)

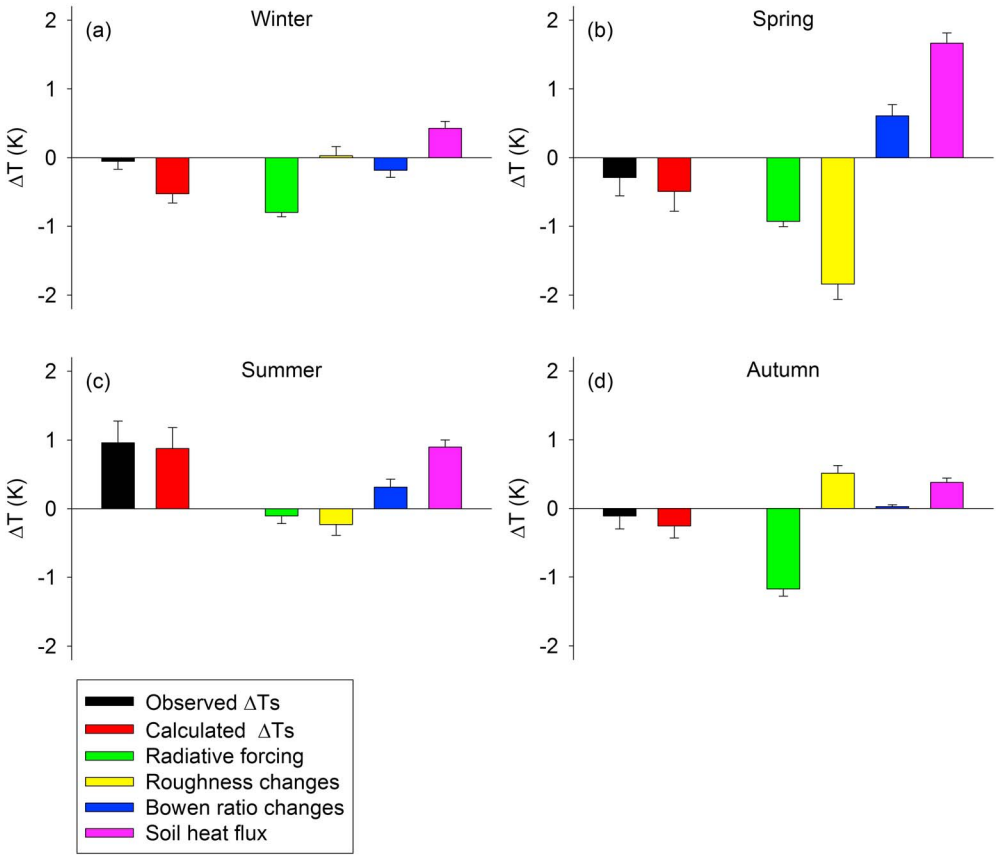

Figure 4. Same as Figure 3 except for nighttime.

and (10). We then fit the daily nighttime r_r by a quadratic function of DOY for each observational period (Table S1). We used these quadratic functions in the ΔT_s partitioning calculation.

Because the air temperature T_a was measured very close to the surface, rather than at the blending height as required by the IBPM theory, the observed difference in T_a between the two sites was largely a result of the biophysical effect of the land use difference. In this study, Term 5 of equation (14) was distributed in proportion to the absolute value of Term 1 to Term 4,

$$\text{Term\_}i' = \text{Term\_}i + \frac{|\,\text{Term\_}i\,|}{\sum_{i=1}^{4}|\,\text{Term\_}i\,|} \times \text{Term 5} \tag{16}$$

where i ranges from 1 to 4, and Term_i' is the refreshed value after distributing Term 5. Unless stated otherwise, the partitioning results presented below have been adjusted according to equation (16).

Half-hourly observations with sensible heat flux between -5 and 5 W m^{-2} were excluded from our analysis in order to avoid division by small numbers in the calculation of r_t from equation (7). The analysis was done separately for daytime and nighttime periods to account for the diurnal asymmetry of the biophysical effect (Schultz et al., 2017).

5. Results and Discussion

5.1. Performance Evaluation of the IBPM Theory

The performance of the IBPM theory is evaluated in both the prognostic mode and the diagnostic mode. Figures 2a and 2b compare the temporal variations in the surface temperature predicted according to equation (4) with the observations at the forest and the shrubland site, respectively, for the spring period. Similar results are obtained for the other three periods. The observed surface to screen height air temperature

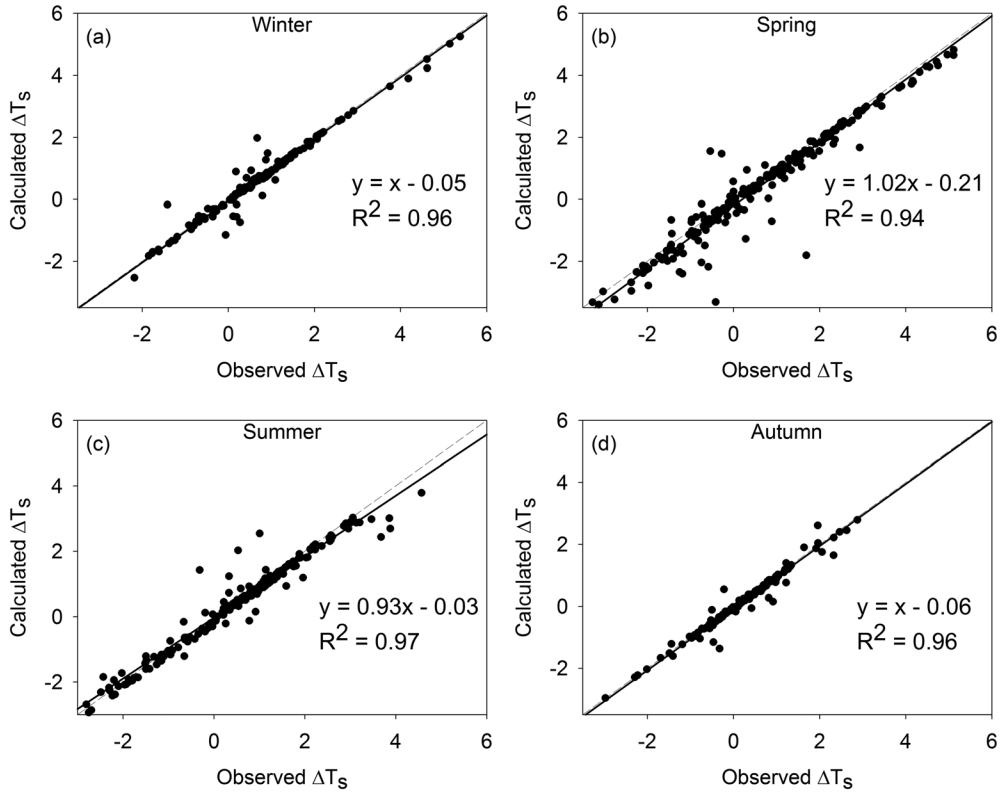

Figure 5. The relationship between half-hour calculated ΔT_s and observed ΔT_s in different seasons for daytime. Results are based on diagnostic application of the IBPM theory. The regression equations and determination coefficients (R^2) were calculated with the geometric mean regression method. The dashed lines represent the 1:1 line, and the solid lines represent the regression results.

difference $T_s - T_a$ have an obvious diurnal pattern. In the nighttime, the value is about −3.4 K and −2.2 K at the forest and the shrub land site, respectively. In the daytime, it increases with time in the morning and decreases in the afternoon, with the maximum value (12.8 ± 1.2 K for the forest, 13.1 ± 1.0 K for shrub; mean ± 1 standard error, hereafter) at 13:00 to 14:00 Beijing time (UTC + 8; 12:00 to 13:00 local solar time). The diagnostic calculation agrees well with the observation, while the prognostic calculation has some bias errors at noon and in the nighttime, especially for the forest site. The mean bias errors of the diagnostic model are −0.1 ± 0.1 K for both sites, and those of the prognostic model are −0.1 ± 0.3 K and −1.1 ± 0.2 K in the daytime, and −3.7 ± 0.5 and −1.1 ± 0.3 at night, for the forest and the shrubland, respectively. Because the prognostic model shows a high uncertainty in predicting the surface temperature, the following analysis is based on the diagnostic model unless stated otherwise.

The seasonal mean surface temperature difference between the shrubland and the forest ΔT_s calculated by the IBPM theory (equation (14)) is in excellent agreement with the observations. The mean bias between calculated and observed ΔT_s is −0.1 K in the daytime. The largest daytime ΔT_s values (both the calculated and observed results) occur in winter and spring, whereas smaller ΔT_s values occur in the summer and fall (Figure 3). The daytime values indicate warmer temperatures over the shrubland compared to the afforested land. The largest calculated and observed nighttime ΔT_s values occur in summer (Figure 4), and the overall agreement is also very good, but mean bias (−0.2 K) is slightly larger in magnitude than the bias in the daytime.

At the half-hour scale, the calculated and the observed daytime ΔT_s follow the 1:1 line in all the seasons, with high determination coefficients ($R^2 > 0.9$; Figure 5). The nighttime results have slightly more scatter but still follow the 1:1 line (R^2 = 0.77 to 0.93; Figures 6b–6d) except during the winter which has a regression slope of 1.2 and R^2 of 0.44 (Figure 6a). These results indicate that omission of higher-order terms in

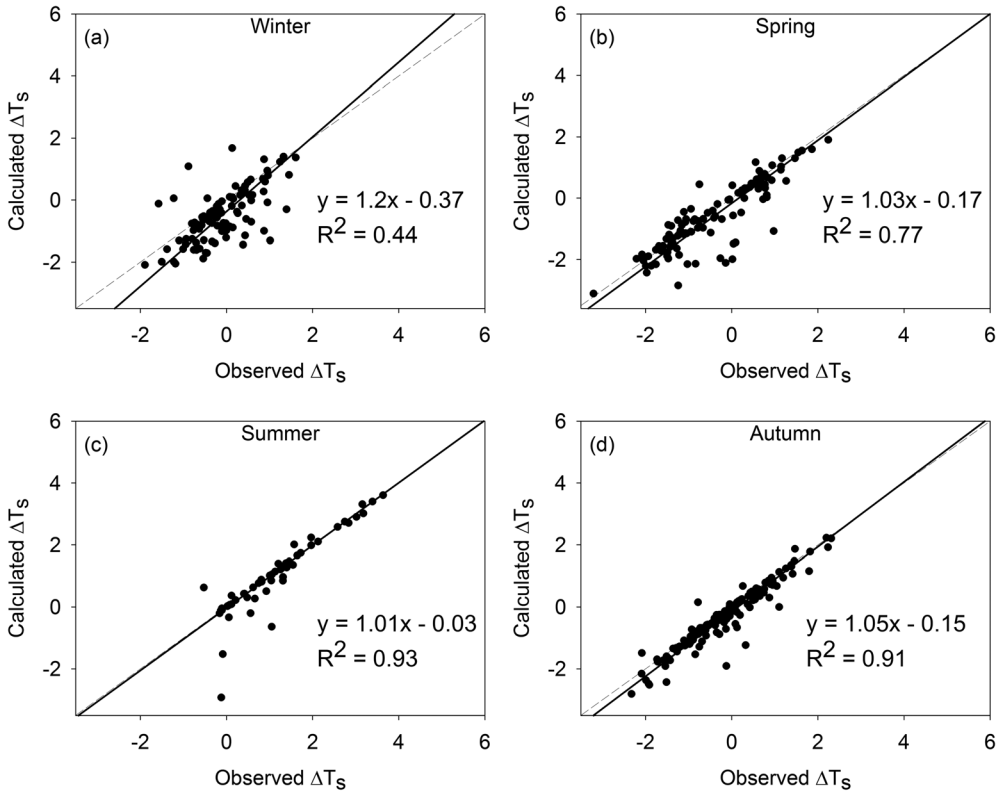

Figure 6. As in Figure 5 except for nighttime.

the derivation of equation (11) is justified and that nonlinear interactions among the individual biophysical drivers is negligible.

5.2. Comparison of Daytime and Nighttime Biophysical Effects

When evaluating the influence of land use change, it is necessary to consider daytime and nighttime periods separately (Lee et al., 2011; Schultz et al., 2017). The daytime and nighttime partitioning of the biophysical effects is presented in Figures 3 and 4. In the daytime, the shrub site is on average 0.5 ± 0.2 K warmer than the forest according to the field observations in the four 10 day periods, while the calculated ΔT_s is 0.4 ± 0.2 K. The warming effect is about half of that given by Peng et al. (2014), who evaluated the influence of afforestation on daytime surface temperature (ΔT_s of 1.1 ± 0.6 K for areas with mean annual precipitation between 400 and 600 mm yr^{-1}) using the MODIS satellite product. In the nighttime, the shrub site is cooler than the forest in the winter, spring, and autumn according to the field observations and the IBPM calculation, with a mean of −0.2 ± 0.1 K to −0.4 ± 0.1 K. In the summer, both the observed ΔT_s (1.0 ± 0.3 K) and calculated ΔT_s (0.9 ± 0.3 K) show that the shrubland is warmer than the forest. According to Peng et al. (2014), the annual mean ΔT_s in the nighttime is about −0.6 ± 0.4 K for areas with the mean annual precipitation between 400 and 600 mm yr^{-1}.

In the daytime, the radiative forcing term (Term 1 on the right-hand side of equation (14)) varies in a small range (0.43–0.92 K) among the four seasons, giving an average ΔT_s value of 0.7 ± 0.1 K (Figure 3, green). This finding is contrary to the previous results, such as in Betts (2000) and Lee et al. (2011), which show that deforestation should lead to a cooling effect because forests generally have lower albedo than open land. In this study, the shrub is denser (mean LAI 0.19) than the forest (mean LAI 0.16), and its leaves and branches are darker than those of the forest (Figure 1). The annual mean albedo is 0.27 at the shrubland and 0.35 at the forest, resulting in a mean ΔS of 29.2 W m^{-2}. If acting alone, the radiative forcing associated with the albedo difference would make the shrub site 0.8 K warmer than the forest; some of this warming is offset by a negative difference in the incoming longwave radiation between the two sites (mean daytime $\Delta L_{\downarrow} = -4.7$ W m^{-2}).

There was no snow cover in our study period. Based on the weather data, there are usually two to three snow events each year in this area and the number of snow cover days is on average less than 7 days. Betts (2000) noted that snow cover can make open land brighter than forests because trees mask snow cover.

In the nighttime, the radiative forcing represents a cooling signal in all the four seasons, with an average value of −0.7 ± 0.2 K (Figure 4, green). The cooling results from the fact that the shrubland receives less incoming longwave radiation than the forest.

The change in surface roughness (Term 2) contributes a warming signal (mean of four seasons 0.3 ± 0.4 K) in the daytime (Figure 3, yellow) but a cooling signal of similar amount (−0.4 ± 0.5 K) in the nighttime (Figure 4, yellow). In the daytime, open lands are less efficient than forests in dissipating heat into the atmospheric boundary layer via turbulent diffusion, and as a result, they warm up faster than forests (Rotenberg & Yakir, 2011). The nighttime cooling signal is consistent with field (Lee et al., 2011; Zhang et al., 2014) and satellite observations (Schultz et al., 2017). At night in stably stratified conditions, open lands are cooler than forests because trees' turbulence brings heat from aloft to the surface (Lee et al., 2011).

Term 3 caused by Bowen ratio changes is 0.1 ± 0.3 K in the daytime (Figure 3, blue) and 0.2 ± 0.2 K in the nighttime. A detailed discussion about this term can be found in section 5.3.

Ground heat flux change (Term 4) has the opposite effect to the radiative forcing in all the four seasons, and its sign is reversed between nighttime and daytime. The mean value of Term 4 is −0.7 ± 0.3 K in the daytime (Figure 3, pink) and 0.8 ± 0.3 K in the nighttime (Figure 4, pink). The difference in G is caused by the different water content and different biomass amount in the topsoil between the two ecosystems. The average soil water content between the 0 to 30 cm depth at the shrub site was 2.9% higher in the winter and autumn and 6.1% higher in the spring and summer of 2006 than that at the forest site. Peng et al. (2014) suggested that part of the surface temperature differences in the nighttime are caused by soil heat capacity changes, but our results show that the temperature changes caused by Term 4 have the opposite sign to the observed ΔT_s when averaged over the four seasons.

5.3. Seasonal Variations of Biophysical Effects

A clear seasonal pattern is seen in the daytime roughness term. In the daytime, surface roughness change (Term 2, Figure 3, yellow) plays a large role and has a similar magnitude (about 0.9 ± 0.2 K) with Term 1 in the winter and the spring period. In these seasons, the shrubland has similar aerodynamic properties to open land because it has lower amounts of aboveground structure. In the summer and the autumn, because the shrub grows faster and has a longer growing season than the forest, its surface roughness is higher than the forest ($\Delta f_1 > 0$), and Term 2 changes its sign and becomes negative in the summer (−0.1 ± 0.2 K) and the autumn (−0.5 ± 0.2 K). At night, the seasonal pattern of this term is not as clear.

The influence of Bowen ratio changes (Term 3) is negligible in the winter and the autumn for both the daytime and the nighttime (Figures 3 and 4). In the spring, the Bowen ratio change causes warming at the shrubland in both the daytime (0.9 ± 0.1 K, Figure 3b) and the nighttime (0.6 ± 0.2 K, Figure 4b). This warming is presumably caused by a lower canopy conductance and a lower transpiration rate, which result in a reduced partitioning of net radiation into the latent heat flux at the shrubland site than at the forest. In the summer, the Bowen ratio change has a cooling effect in the daytime (−0.4 ± 0.3 K, Figure 3c) and a warming effect in the nighttime (0.3 ± 0.1 K, Figure 4c). Our result shows that the effect caused by Bowen ratio change is related to the growing status of the two ecosystems. The higher influences occur in the spring and the summer than in the other two seasons.

We have also applied the partitioning of the biophysical effects in the winter and summer in 2008 (Figure S1). The results show that the ΔT_s values and influences of these biophysical factors have the same signs and similar magnitudes as the results obtained for 2006, confirming that our partitioning method is robust and that our results are not affected by the short duration (10 days) chosen for each season.

5.4. Improvements Over the Original IBPM Theory

The original IBPM theory proposed by Lee et al. (2011) is based on the ideal condition that two adjacent ecosystems share the same background atmospheric state, including air temperature (T_a) and incoming longwave radiation ($L_\downarrow$). In actual field observations, these variables may be different between paired sites. For example, Chen and Dirmeyer (2016) considered the differences between air temperature in their IBPM

analysis. Their results showed that the air temperature difference is about 0.7 K in the daytime and −0.8 K in the nighttime for eight FLUXNET site pairs.

In the present study, the air temperature term (Term 5, equation (14)) is on average 0.4 ± 0.1 K in the daytime and −0.8 ± 0.1 K in the nighttime (Term 5, Figures S2 and S3, gray). The largest contribution (−1.7 ± 0.1 K) occurs in the autumn at night (Figure S3d). The temperature term consists of two parts, the actual air temperature difference ΔT_a and a part resulting from differentiation of the apparent net radiation (equation (14)). The first part is dominant. For example, in Figure S3d (autumn, nighttime), these two parts are equal to −2.3 K and 0.6 K, respectively.

If we exclude the air temperature term from equation (14), the calculated ΔT_s will deviate significantly from the observations (Figures S4 and S5). However, this term itself is not a biophysical driver and instead should be interpreted as a result of the biophysical effect. In the IBPM framework, the biophysical effect of land use is measured by changes in the surface temperature (ΔT_s). This effect will also influence the air temperature very close to the surface. (Only at the blending height and above is air temperature insensitive to the land use change.) For this reason, in Figures 3 and 4, we have distributed the temperature term into the other four biophysical contributions.

The second modification to the IBPM theory is the inclusion of the incoming longwave radiation change ($\Delta L_\downarrow$) in the radiative forcing term (Term 1, equation (14)). In the present study, the mean $\Delta L_\downarrow$ is −5.8 W m^{-2}. The difference in the incoming longwave radiation between the two sites contributes −0.2 ± 0.1 K and −0.7 ± 0.2 K to the daytime and nighttime ΔT_s, respectively. If $\Delta L_\downarrow$ is excluded from equation (14), the agreement between the calculated and the observed ΔT_s will degrade, especially for the nighttime (Figures S6 and S7). The average R^2 changes from 0.96 to 0.88 with and without $\Delta L_\downarrow$, respectively, for the daytime, and decreases from 0.76 to 0.47 for the nighttime. Other researchers have noted the differences in $L_\downarrow$ between adjacent sites (Broucke et al., 2015; Chen & Dirmeyer, 2016; Juang et al., 2007; Lee et al., 2011). In their investigation of climatic effects, this difference is ignored by Juang et al. (2007) and Lee et al. (2011) and is included by Chen and Dirmeyer (2016) and Broucke et al. (2015). In the study of Chen and Dirmeyer (2016), the differences in $\Delta L_\downarrow$ ranges from −24 to 12 W m^{-2}, and its mean contribution to the nighttime ΔT_s is small (0 ± 0.1 K). Broucke et al. (2015) pointed out that the incoming longwave radiation change is not accurately simulated by climate models, which may result in biases in modeling investigation of the biophysical effects of land use change. They attributed the difference in the nighttime $L_\downarrow$ to higher water vapor, aerosol loading, and warmer air at the forest site than in the adjacent open land. Some of the aerosols over the forest can be secondary organic aerosols formed from biogenic volatile organic compounds emitted by trees (Claeys et al., 2004). We found that $\Delta L_\downarrow$ has a significant positive relationship with ΔT_a, with a Pearson's correlation coefficient 0.45 ($p < 0.01$). Thus, we infer that the negative $\Delta L_\downarrow$ is partially related to the warmer air at the forest site.

5.5. Diagnostic Versus Prognostic Application

The results shown in Figures 3–6 are based on the diagnostic application of the IBPM theory, whereby the observed sensible heat flux, air temperature, and surface temperature were used to determine the total heat resistance at the shrubland and the forest site. When the resistance is determined with the parameterization equations (equations (8)–(10)) as in a prognostic application, the calculated ΔT_s shows poorer agreement with the observations (Figures S8 and S9), with R^2 reductions from 0.94–0.97 (Figure 5) to 0.06–0.20 for the daytime (Figure S8) and from 0.44–0.93 (Figure 6) to 0.01–0.28 for the nighttime (Figure S9). The major uncertainty comes from the calculation of radiometric resistance (r_r). In the current study, the daytime r_r is expressed as an exponential function of LAI (Zhao et al., 2016) and the nighttime r_r is a quadratic function of DOY. The daytime r_r calculated from LAI is constant in a day without any diurnal change. According to Figure 2, large bias errors of the prognostic calculation happen at noon, implying that the actual r_r around noon is different from the rest of the daytime hours.

The mean values of the predicted r_a, r_{ex}, and r_r for the shrubland site and the forest site are listed in Table S2. The prognostic calculation captures the temporal pattern observed at the shrub land site in the nighttime for most days (Figure 2b), but the result for the forest site is not as satisfactory (Figure 2a). Because r_r is the dominant resistance in the nighttime, the partition calculation is very sensitive to uncertainties in r_r. In future studies, it is necessary to find better methods to predict r_r for successful prognostic applications.

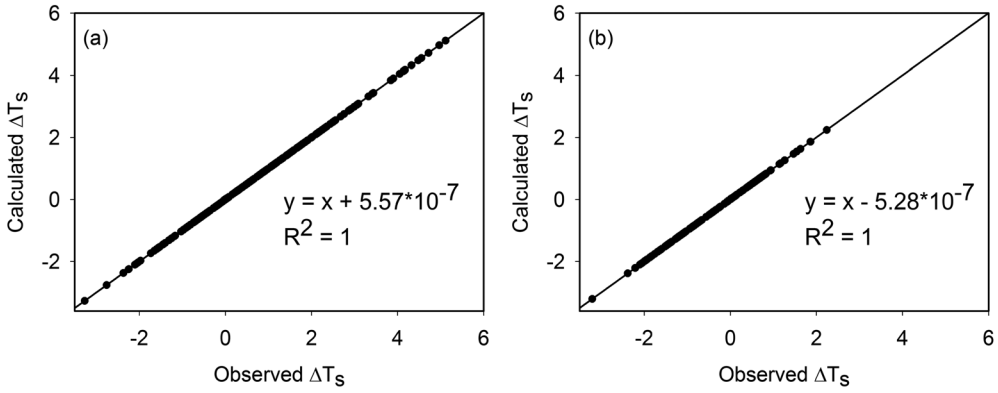

Figure 7. Relationship between half-hour calculated ΔT_s and observed ΔT_s for (a) spring daytime and (b) spring nighttime periods. Results are based on the DTM theory. The regression equations and determination coefficients (R^2) were calculated with the geometric mean regression method. The dashed lines represent the 1:1 line, and the solid lines represent the regression results.

The energy redistribution factor (*f*) values from the diagnostic application (Table S3) are consistent with published results. The 24 h mean value is 4.4 for the forest and 4.8 for the shrubland. The daytime values, ranging from 5.3 to 8.0, are higher than those in the nighttime (1.2 to 2.1). Bright et al. (2017) calculated the annual mean *f* of 13 deciduous broadleaf forests using the FLUXNET data, giving a mean value of 3.8. Their semimechanistic model yields a prediction of *f* from 4.1 to 6.5 for the deciduous broadleaf forests around 40°N. Cao et al. (2016) reported a mean nighttime *f* of 1.3 ± 0.8 in the semiarid region in China.

In a critique of the IBPM theory, Rigden and Li (2017) suggest that the IBPM may overestimate the contributions due to roughness change by 10–25% because of a cross correlation of the aerodynamic resistance with Bowen ratio. Their analysis is based on the Monin-Obukhov parameterization of the resistance term. We did not verify if such correlation exists at our sites. However, because in the present study albedo changes and incoming longwave radiation changes are the dominant factors in the daytime and the nighttime, respectively, this correlation would not affect our general conclusions.

5.6. Comparison of IBMP and DTM

The half-hourly ΔT_s calculated with the DTM method is in perfect agreement with the observations (Figure 7). Under the constraint of energy balance, the only assumption involved in the DTM is the Taylor expansion of

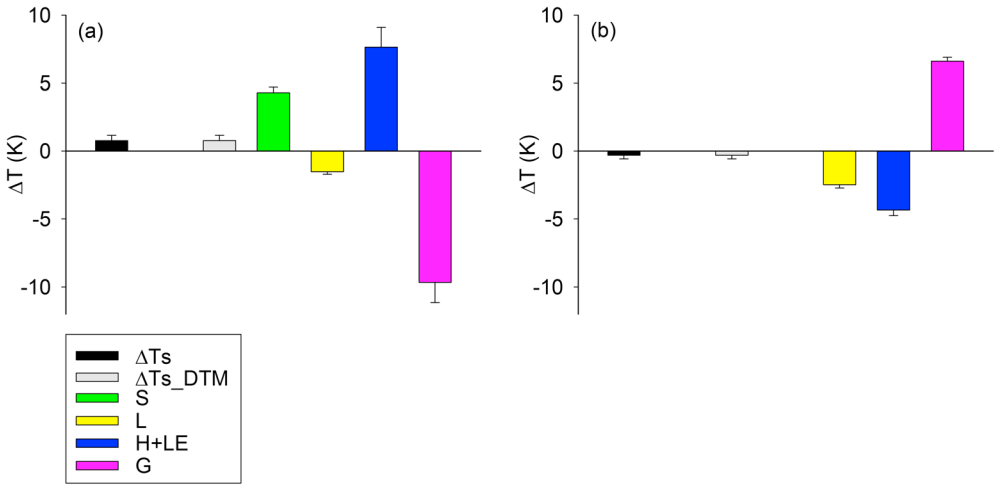

Figure 8. Partition of the biophysical effects in the spring according to the DTM theory in (a) daytime and (b) nighttime. Error bars are given as 1 SE. Black bars denote observed ΔT_s, gray bars denote the ΔT_s calculated by the DTM theory, green bars denote shortwave radiative forcing, yellow bars denote incoming longwave radiation changes, blue bars denote sensible heat and latent heat changes, and pink bars denote the soil heat flux changes.

Table 2
Observed ΔT_s (K) and Calculated ΔT_s (K) Without Energy Balance Closure Correction

	Season	ΔT_s observed	ΔT_s IBPM	ΔT_s DTM	Slope	Intercept	R^2
Day	Winter	0.77 ± 0.23	−0.40 ± 0.42	−1.11 ± 0.74	2.04 ± 0.22	−1.95 ± 0.16	0.11
	Spring	0.74 ± 0.42	−0.31 ± 0.52	−0.30 ± 0.64	1.73 ± 0.17	−1.62 ± 0.13	0.14
	Summer	0.19 ± 0.46	0.25 ± 0.38	0.16 ± 0.60	1.08 ± 0.14	0.00 ± 0.03	0.12
	Autumn	0.21 ± 0.22	−0.43 ± 0.21	−1.26 ± 0.60	1.87 ± 0.22	−0.81 ± 0.04	0.05
Night	Winter	−0.05 ± 0.11	0.04 ± 0.49	2.86 ± 0.58	2.78 ± 0.28	0.87 ± 0.07	0.19
	Spring	−0.29 ± 0.27	2.93 ± 0.52	5.02 ± 0.38	2.10 ± 0.23	3.79 ± 0.07	0.14
	Summer	0.96 ± 0.31	1.71 ± 0.15	3.18 ± 0.32	1.62 ± 0.25	0.34 ± 0.23	0.23
	Autumn	−0.11 ± 0.19	0.87 ± 0.25	1.09 ± 0.34	1.89 ± 0.21	1.00 ± 0.01	0.19

Note. Regression parameters for IBPM are calculated based on half-hour results (mean ± 1 standard error).

the Stephan-Boltzmann expression (equation (2)). In the supporting information, we have shown mathematically why addition of the component contributions should be exactly the same as the observed ΔT_s. In Juang et al. (2007), the calculated ΔT_s with the DTM method is 0.5 K lower than the observed value, due in part to the omission of $\Delta L_{\downarrow}$ in their calculation.

The DTM partitioning of the biophysical effects is shown in Figure 8 for the spring and in Figures S10 and S11 for the other seasons. In the spring, the calculated and the observed ΔT_s are 0.7 ± 0.4 K in the daytime and −0.3 ± 0.3 K in the nighttime. According to the DTM theory, some of the component contributions are an order of magnitude greater than the total biophysical signal itself. For example, the shortwave radiative forcing results in a contribution of 4.3 ± 0.4 K to the surface temperature change in the daytime. Similarly, in Broucke et al. (2015), the daytime radiative forcing associated with albedo change contributes about 5 K and the biophysical effect associated with changes in *H* and LE is more than 10 K. In contrast, the component contributions calculated with the IBPM theory are on the same order of magnitude as the total biophysical signal (Figures 3 and 4).

In the daytime, the sum of first two terms in DTM (equation (2)), representing local radiative forcing, has the same sign with Term 1 of IBPM, as does the fourth term (representing ground heat flux changes) in DTM with Term 4 of IBPM. But the absolute values are 6 to 9 times higher than the related terms of IBPM. The situation is similar in the nighttime. The influences of radiative forcing changes and ground heat flux changes calculated with the two theories show similar diurnal and seasonal patterns. After removing the influences of radiative forcing changes and ground heat flux changes, the residual terms in DTM (the third term in equation (2), representing the influence of sensible heat and latent heat changes) should be comparable to the residual terms in IBPM (Term 2 and Term 3, representing the role of energy redistribution associated with roughness change and with Bowen ratio change). In most cases, these residual terms also show similar signs and seasonal pattern except in the autumn at night, which is caused by a stronger influence of air temperature in this period.

The major difference between the two theories is that the DTM theory provides a total evaluation of "an ecophysiological and aerodynamic component" via the third term in equation (2) (Juang et al., 2007), while the IBPM divides this term into two intrinsic biophysical factors (Δr_t and $\Delta\beta$) by introducing an energy redistribution factor (*f*). In a refinement of the DTM theory, Luyssaert et al. (2014) have also divided the third term in equation (2) into sensible heat changes and latent heat changes, but because these two terms themselves are functions of the surface temperature, they are not independent of each other. For this reason, DTM is not suitable for single-factor perturbation analysis. For example, the IBPM theory has been used successfully to predict the surface temperature change caused by albedo change associated with replacement of conventional roofs with reflective materials in urban environments (Zhao et al., 2017). If we use the DTM theory for this analysis, by retaining only the albedo term in equation (2), the predicted temperature change will be too large in magnitude.

5.7. The Importance of Energy Balance Closure

We investigated the relationship between the calculated ΔT_s and the observed ΔT_s under energy imbalance conditions. Table 2 shows the regression parameters of the IBPM results using the original sensible heat and

latent heat measurements before energy balance correction. The calculated ΔT_s and the observed ΔT_s show poor agreement and are even opposite in sign. The half-hourly results deviate greatly from 1:1 line with lower R^2 values especially in the nighttime (Figures S12 and S13).

The DTM results are also sensitive to biases in the energy balance components. According to the DTM calculation, the mean ΔT_s is -0.6 ± 0.3 K in the daytime and -3.0 ± 0.8 K in the nighttime in our study periods. For comparison, the observed daytime and nighttime are 0.5 ± 0.2 K and 0.1 ± 0.3 K, respectively. At the half-hourly scale, the DTM-calculated ΔT_s departs more severely from the observations (Figures S14 and S15) than the IBPM results (Figures S12 and S13). The lack of energy balance may explain the DTM bias errors reported by other researchers. For example, Broucke et al. (2015) used a refined DTM equation, and 17%–64% of their results have bias errors larger than 2 K. For their paired-site observations, they reported that the energy imbalance is about 11 W m^{-2}. On the other hand, by applying the same energy balance adjustment as in the present study, Chen and Dirmeyer (2016) showed that the annual mean ΔT_s calculated with DTM is in close agreement with FLUNET observations.

6. Conclusions

In this study, a modified theory of the IBPM is used to investigate the biophysical effects on the surface temperature caused by afforestation in the Kubuqi Desert. We find that the afforestation activity in this dryland landscape has a cooling effect (-0.5 ± 0.2 K) in the daytime in all the seasons and a warming effect (0.2 ± 0.1 K) in the nighttime during the winter, spring, and autumn but a cooling effect (-1.0 ± 0.3 K) in the summer. The daytime cooling effect is partly attributed to the fact that the forested site has a higher albedo than the reference shrubland site. The roles of roughness and Bowen ratio changes are variable between seasons and between daytime and nighttime. Afforestation also causes ground heat flux changes, which has a warming effect (0.7 ± 0.3 K) in the daytime and cooling effect (-0.8 ± 0.3 K) in the nighttime.

Generally, both the IBPM and DTM theory show that the albedo changes contribute most to the surface temperature change in the daytime, and the incoming longwave radiation changes contribute most in the nighttime. Contributions caused by ground heat flux changes have opposite signs to the surface temperature changes, offsetting the other terms. Contributions of roughness and Bowen ratio changes (or H and LE changes in DTM) show larger seasonal variations than other terms.

The modified IBPM theory agrees very well with the observed temporal variations in the surface temperature and with the observed temperature difference ΔT_s between the paired sites at the half-hourly time scale. Compared with the original IBPM theory, this modified version takes into account the incoming longwave radiation and air temperature differences between the sites. However, the performance of the prognostic model is not as good as that of the diagnostic model due to the complexity of r_r estimation, an issue that needs to be investigated in the future.

The decomposition results of the DTM theory are broadly consistent with those obtained with the IBPM theory. Because DTM gives the same weight to each of the energy balance components without separating the external forcing and energy redistribution processes, some of the partitioned component contributions are about an order of magnitude greater in magnitude than the observed ΔT_s. In comparison, the component contributions calculated with the IBPM theory are similar in magnitude to the observed ΔT_s.

Energy balance closure is an important condition for both the IBPM and the DTM theory. If energy imbalance is not corrected properly, the calculated temperature difference will greatly depart from the observed value, especially for the DTM theory.

Acknowledgments
This work is supported jointly by the Department of Earth System Science, Tsinghua University, and the School of Forestry and Environmental Studies, Yale University. We are grateful for the financial support from National Basic Research Program of China (2013CB956601) and China Scholarship Council. We thank Long Wei and all the staff involved in data collection and processing. We also thank Elion Resources Group, Inc., for the logistic help during our field measurements. All the data used in this study are available at the Zenodo website (https://doi.org/10.5281/zenodo.1137738) or on request from the corresponding author (xuhui.lee@yale.edu).

References

Bala, G., Caldeira, K., Wickett, M., Phillips, T. J., Lobell, D. B., Delire, C., & Mirin, A. (2007). Combined climate and carbon-cycle effects of large-scale deforestation. *Proceedings of the National Academy of Sciences of the United States of America*, *104*(16), 6550–6555. https://doi.org/10.1073/pnas.0608998104

Betts, R. A. (2000). Offset of the potential carbon sink from boreal forestation by decreases in surface albedo. *Nature*, *408*(6809), 187–190. https://doi.org/10.1038/35041545

Bonan, G. B. (2008). Forests and climate change: Forcings, feedbacks, and the climate benefits of forests. *Science*, *320*(5882), 1444–1449. https://doi.org/10.1126/science.1155121

Bonan, G. B., Pollard, D., & Thompson, S. L. (1992). Effects of boreal forest vegetation on global climate. *Nature*, *359*(6397), 716–718. https://doi.org/10.1038/359716a0

Bright, R. M., Anton-Fernandez, C., Astrup, R., Cherubini, F., Kvalevag, M., & Stromman, A. H. (2014). Climate change implications of shifting forest management strategy in a boreal forest ecosystem of Norway. *Global Change Biology*, *20*(2), 607–621. https://doi.org/10.1111/gcb.12451

Bright, E. D., O'Halloran, T., Pongratz, J., Zhao, K., & Cescatti, A. (2017). Local temperature response to land cover and management change driven by non-radiative processes. *Nature Climate Change*, *7*(4), 296–302. https://doi.org/10.1038/nclimate3250

Broucke, S., Luyssaert, S., Davin, E. L., Janssens, I., & van Lipzig, N. (2015). New insights in the capability of climate models to simulate the impact of LUC based on temperature decomposition of paired site observations. *Journal of Geophysical Research: Atmospheres*, *120*, 5417–5436. https://doi.org/10.1002/2015JD023095

Burakowski, E., Tawfik, A., Ouimette, A., Lepine, L., Novick, K., Ollinger, S., … Bonan, G. (2018). The role of surface roughness, albedo, and Bowen ratio on ecosystem energy balance in the eastern United States. *Agricultural and Forest Meteorology*, *249*, 367–376. https://doi.org/10.1016/j.agrformet.2017.11.030

Businger, J. A. (1988). A note on the Businger-Dyer profiles. *Boundary-Layer Meteorology*, *42*(1-2), 145–151. https://doi.org/10.1007/Bf00119880

Cao, C., Lee, X., Liu, S., Schultz, N., Xiao, W., Zhang, M., & Zhao, L. (2016) Urban heat islands in China enhanced by haze pollution. *Nature Communications*, *7*, 12509. https://doi.org/10.1038/ncomms12509

Chen, L., & Dirmeyer, P. A. (2016). Adapting observationally based metrics of biogeophysical feedbacks from land cover/land use change to climate modeling. *Environmental Research Letters*, *11*(3). https://doi.org/10.1088/1748-9326/11/3/034002

Chirino, E., Bonet, A., Bellot, J., & Sanchez, J. R. (2006). Effects of 30-year-old Aleppo pine plantations on runoff, soil erosion, and plant diversity in a semi-arid landscape in south eastem Spain. *Catena*, *65*(1), 19–29. https://doi.org/10.1016/j.catena.2005.09.003

Claeys, M., Graham, B., Vas, G., Wang, W., Vermeylen, R., Pashynska, V., … Maenhaut, W. (2004). Formation of secondary organic aerosols through photooxidation of isoprene. *Science*, *303*(5661), 1173–1176. https://doi.org/10.1126/science.1092805

Davin, E. L., & de Noblet-Ducoudre, N. (2010). Climatic impact of global-scale deforestation: Radiative versus nonradiative processes. *Journal of Climate*, *23*(1), 97–112. https://doi.org/10.1175/2009JCLI3102.1

Grunzweig, J. M., Gelfand, I., Fried, Y., & Yakir, D. (2007). Biogeochemical factors contributing to enhanced carbon storage following afforestation of a semi-arid shrubland. *Biogeosciences*, *4*(5), 891–904. https://doi.org/10.5194/bg-4-891-2007

Holtsmark, B. (2012). Harvesting in boreal forests and the biofuel carbon debt. *Climatic Change*, *112*(2), 415–428. https://doi.org/10.1007/s10584-011-0222-6

Hudiburg, T. W., Law, B. E., Wirth, C., & Luyssaert, S. (2011). Regional carbon dioxide implications of forest bioenergy production. *Nature Climate Change*, *1*(8), 419–423. https://doi.org/10.1038/nclimate1264

Jia, X., Fu, B., Feng, X., Hou, G., Liu, Y., & Wang, X. (2014). The tradeoff and synergy between ecosystem services in the grain-for-green areas in northern Shaanxi, China. *Ecological Indicators*, *43*, 103–113. https://doi.org/10.1016/j.ecolind.2014.02.028

Juang, J. Y., Katul, G., Siqueira, M., Stoy, P., & Novick, K. (2007). Separating the effects of albedo from eco-physiological changes on surface temperature along a successional chronosequence in the southeastern United States. *Geophysical Research Letters*, *34*, L21408. https://doi.org/10.1029/2007GL031296

Lee, X., Goulden, M. L., Hollinger, D. Y., Barr, A., Black, T. A., Bohrer, G., … Zhao, L. (2011). Observed increase in local cooling effect of deforestation at higher latitudes. *Nature*, *479*(7373), 384–387. https://doi.org/10.1038/nature10588

Lhomme, J. P., Katerji, N., Perrier, A., & Bertolini, J. M. (1988). Radiative surface-temperature and convective flux calculation over crop canopies. *Boundary-Layer Meteorology*, *43*(4), 383–392. https://doi.org/10.1007/Bf00121714

Li, M. M., Liu, A. T., Zou, C. J., Xu, W. D., Shimizu, H., & Wang, K. Y. (2012). An overview of the "Three-North" Shelterbelt project in China. *Forestry Studies China*, *14*(1), 70–79. https://doi.org/10.1007/s11632-012-0108-3

Luyssaert, S., Jammet, M., Stoy, P. C., Estel, S., Pongratz, J., Ceschia, E., … Dolman, A. J. (2014). Land management and land-cover change have impacts of similar magnitude on surface temperature. *Nature Climate Change*, *4*(5), 389–393. https://doi.org/10.1038/nclimate2196

Mahmood, R., Pielke, R. A. Sr., Hubbard, K. G., Niyogi, D., Dirmeyer, P. A., McAlpine, C., … Fall, S. (2014). Land cover changes and their biogeophysical effects on climate. *International Journal of Climatology*, *34*(4), 929–953. https://doi.org/10.1002/joc.3736

Nosetto, M. D., Jobbagy, E. G., & Paruelo, J. M. (2006). Carbon sequestration in semi-arid rangelands: Comparison of *Pinus ponderosa* plantations and grazing exclusion in NW Patagonia. *Journal of Arid Environments*, *67*(1), 142–156. https://doi.org/10.1016/j.jaridenv.2005.12.008

Peng, S. S., Piao, S. L., Zeng, Z. Z., Ciais, P., Zhou, L. M., Li, L. Z. X., … Zeng, H. (2014). Afforestation in China cools local land surface temperature. *Proceedings of the National Academy of Sciences of the United States of America*, *111*(8), 2915–2919. https://doi.org/10.1073/pnas.1315126111

Rigden, A. J., & Li, D. (2017). Attribution of surface temperature anomalies induced by land use and land cover changes. *Geophysical Research Letters*, *44*, 6814–6822. https://doi.org/10.1002/2017GL073811

Rotenberg, E., & Yakir, D. (2011). Distinct patterns of changes in surface energy budget associated with forestation in the semiarid region. *Global Change Biology*, *17*(4), 1536–1548. https://doi.org/10.1111/j.1365-2486.2010.02320.x

Sartori, F., Lal, R., Ebinger, M. H., & Eaton, J. A. (2007). Changes in soil carbon and nutrient pools along a chronosequence of poplar plantations in the Columbia Plateau, Oregon, USA. *Agriculture, Ecosystems & Environment*, *122*(3), 325–339. https://doi.org/10.1016/j.agee.2007.01.026

Schultz, N. M., Lawrence, P. J., & Lee, X. (2017). Global satellite data highlights the diurnal asymmetry of the surface temperature response to deforestation. *Journal of Geophysical Research: Biogeosciences*, *122*, 903–917. https://doi.org/10.1002/2016JG003653

State Forestry Administration of the People's Republic of China (2013). Eighth National Forest Resource Inventory Report (2009–2013). Retrieved from http://211.167.243.162:8085/8/chengguobaogao/showpageinit. (Accessed in June 2017).

Stewart, J. B., Kustas, W. P., Humes, K. S., Nichols, W. D., Moran, M. S., & De Bruin, H. (1994). Sensible heat flux-radiometric surface temperature relationship for eight semiarid areas. *Journal of Applied Meteorology*, *33*(9), 1110–1117. https://doi.org/10.1175/1520-0450(1994)033%3C1110:SHFRST%3E2.0.CO;2

Twine, T. E., Kustas, W. P., Norman, J. M., Cook, D. R., Houser, P. R., Meyers, T. P., … Wesely, M. L. (2000). Correcting eddy-covariance flux underestimates over a grassland. *Agricultural and Forest Meteorology*, *103*(3), 279–300. https://doi.org/10.1016/S0168-1923(00)00123-4

Webb, E. K., Pearman, G. I., & Leuning, R. (1980). Correction of flux measurements for density effects due to heat and water vapour transfer. *Quarterly Journal of the Royal Meteorological Society*, *106*(447), 85–100. https://doi.org/10.1002/qj.49710644707

Wilczak, J. M., Oncley, S. P., & Stage, S. A. (2001). Sonic anemometer tilt correction algorithms. *Boundary-Layer Meteorology*, *99*(1), 127–150. https://doi.org/10.1023/A:1018966204465

Wu, Z., Wu, J., Liu, J., He, B., Lei, T., & Wang, Q. (2013). Increasing terrestrial vegetation activity of ecological restoration program in the Beijing–Tianjin Sand Source Region of China. *Ecological Engineering*, *52*, 37–50. https://doi.org/10.1016/j.ecoleng.2012.12.040

Zhang, M., Lee, X., Yu, G., Han, S., Wang, H., Yan, J., … Hirano, T. (2014). Response of surface air temperature to small-scale land clearing across latitudes. *Environmental Research Letters*, *9*(3), 034002. https://doi.org/10.1088/1748-9326/9/3/034002

Zhang, Y., Peng, C., Li, W., Tian, L., Zhu, Q., Chen, H., … Xiao, X. (2016). Multiple afforestation programs accelerate the greenness in the 'Three North' region of China from 1982 to 2013. *Ecological Indicators*, *61*, 404–412. https://doi.org/10.1016/j.ecolind.2015.09.041

Zhao, L., Lee, X., Smith, R. B., & Oleson, K. (2014). Strong contributions of local background climate to urban heat islands. *Nature*, *511*(7508), 216–219. https://doi.org/10.1038/nature13462

Zhao, L., Lee, X., Suyker, A. E., & Wen, X. (2016). Influence of leaf area index on the radiometric resistance to heat transfer. *Boundary-Layer Meteorology*, *158*(1), 105–123. https://doi.org/10.1007/s10546-015-0070-4

Zhao, L., Lee, X., & Schultz, N. (2017). A wedge strategy for mitigation of urban warming in future climate scenarios. *Atmospheric Chemistry and Physics Discussions*, *2017*, 1–28. https://doi.org/10.5194/acp-2016-1046